

Proper Motion of the Draco Dwarf Galaxy Based On *Hubble Space Telescope* Imaging.¹

Carlton Pryor

*Dept. of Physics and Astronomy, Rutgers, the State University of New Jersey,
136 Frelinghuysen Rd., Piscataway, NJ 08854-8019*

E-mail address: pryor@physics.rutgers.edu

Slawomir Piatek

Dept. of Physics, New Jersey Institute of Technology, Newark, NJ 07102

E-mail address: piatek@physics.rutgers.edu

Edward W. Olszewski

Steward Observatory, The University of Arizona, Tucson, AZ 85721

E-mail address: eolszewski@as.arizona.edu

ABSTRACT

We have measured the proper motion of the Draco dwarf galaxy using images at two epochs with a time baseline of about two years taken with the Hubble Space Telescope and the Advanced Camera for Surveys. Wide Field Channel 1 and 2 provide two adjacent fields, each containing a known QSO. The zero point for the proper motion is determined using both background galaxies and the QSOs and the two methods produce consistent measurements within each field. Averaging the results from the two fields gives a proper motion in the equatorial coordinate system of $(\mu_\alpha, \mu_\delta) = (17.7 \pm 6.3, -22.1 \pm 6.3)$ mas century⁻¹ and in the Galactic coordinate system of $(\mu_\ell, \mu_b) = (-23.1 \pm 6.3, -16.3 \pm 6.3)$ mas century⁻¹. Removing the contributions of the motion of the Sun and of the LSR to the measured proper motion yields a Galactic rest-frame proper motion of $(\mu_\alpha^{\text{Grf}}, \mu_\delta^{\text{Grf}}) = (51.4 \pm 6.3, -18.7 \pm 6.3)$ mas century⁻¹ and $(\mu_\ell^{\text{Grf}}, \mu_b^{\text{Grf}}) = (-21.8 \pm 6.3, -50.1 \pm 6.3)$ mas century⁻¹. The implied space velocity with respect to the Galactic center is $(\Pi, \Theta, Z) = (27 \pm 14, 89 \pm 25, -212 \pm 20)$ km s⁻¹. This velocity implies that the orbital inclination is 70°, with a 95% confidence interval of (59°, 80°), and that the plane of the orbit is consistent with that of the vast polar structure (VPOS) of Galactic satellite galaxies.

Subject headings: galaxies: dwarf spheroidal — galaxies: individual (Draco) — astrometry: proper motion

1. Introduction

The *Hubble Space Telescope* (HST) has proven to be an excellent instrument for astrometry and, in particular, for measuring absolute proper motions of Galactic globular clusters (*e.g.*, Milone et al. 2006), Galactic satellite galaxies (*e.g.*, Sohn et al. 2013, and references therein), and even the more distant galaxy M31 (Sohn et al. 2012). The measurement methods have been evolving alongside the successive generations of detectors on HST and the discovery of additional dwarf galaxies in the vicinity of the Milky Way. These measurements require the presence of at least one object in the science field with a known or negligibly small absolute proper motion that serves as a standard of rest. The published absolute proper motions of Galactic globular clusters and dwarf galaxies using HST data use three types of standards of rest: QSOs, resolved compact background galaxies, and foreground stellar populations. Each of these has advantages and disadvantages which are discussed below.

Piatek et al. (2002b) reports the first successful measurement of an absolute proper motion for Fornax using HST data employing spectroscopically-confirmed QSOs as standards of rest. The advantage of using a QSO is that it is typically sufficiently distant that its PSF is the same as that of a star and yet it is bright enough to be among the brighter objects in the field. Thus, a single—empirically derived—effective point spread function (Anderson & King 2000, ePSF) determines the locations of stars and the QSO. However, there are weaknesses to this method. 1) The scarcity of suitable QSOs, which forces the science field to be centered on the location of the QSO and not on the highest stellar surface density of the target galaxy or globular cluster. 2) The uncertainty in the position of a single object, the QSO, primarily determines the uncertainty in the measured proper motion, if there are enough stars of the target (typically more than 20) in the field. 3) If the QSO is too bright compared to the stars of the target, the exposure time may be too short to yield a large enough sample of stars to measure the proper motion. 4) If the QSO is too faint compared to the stars of the target, the proper motion is poorly determined even if there are many stars with high S/N in the sample (see item 2 above). 5) Using QSOs requires considerable preparatory effort to find QSO candidates in a deep color-magnitude diagram and then spectroscopically confirm them. 6) If a target has no suitable background QSOs, its absolute proper motion cannot ever be measured with this method. 7) A typical QSO is bluer than a typical star, causing their PSFs to potentially differ despite their point-like images.

¹Based on observations with the NASA/ESA *Hubble Space Telescope*, obtained at the Space Telescope Science Institute, which is operated by the Association of Universities for Research in Astronomy, Inc., under NASA contract NAS 5-26555. The observations are associated with programs 10229 and 10812.

As the exposure time increases, an HST image reveals an increasing number of distant galaxies, some with compact, almost point-like, cores. Together, these compact galaxies can act as a standard of rest as shown by Mahmud & Anderson (2008). Although the uncertainty in the position of a single compact-core galaxy is likely to be worse than that of a QSO, an average position for tens, or even hundreds, of galaxies can yield an uncertainty that is comparable to or even better than that for a QSO. Mahmud & Anderson (2008) and Sohn et al. (2010) have developed a method of using galaxies as the standard of rest, which has been applied to derive the proper motion of, for example, Leo II (Lépine et al. 2011), M31 (Sohn et al. 2012), and Leo I (Sohn et al. 2013). The advantage of this method is a complete freedom in placing an HST camera field in the target. This freedom either allows the second-epoch observations to be paired with already-existing deep first-epoch observations meant for photometry and stellar population studies (*e.g.*, Sohn et al. 2013), which is a good use of existing resources, or allows placing the field at or very close to the center of the target to maximize the number of member stars. However, the method has weaknesses. 1) The exposure time per frame must be long, Sohn et al. (2013) use about 1,500 s, in order for there to be enough compact-core galaxies with a high enough S/N to establish an accurate zero point. 2) Automated identification of compact-core galaxies does not work efficiently. The process misidentifies as galaxies image artifacts, close stellar pairs, and superpositions of a star on nebula or a galaxy. Because the method requires a “clean” sample, the selection must be supported by human judgment. 3) The most compact galaxies (*e.g.*, AGN) may have an ePSF that differs only subtly from that of a star, so these ideal reference objects may be rejected by both automated selection criteria and visual inspection. 4) A galaxy is a resolved object having a unique morphology. Using a stellar ePSF to determine its “center of light” can lead to large systematic and random errors. Instead, the position of each galaxy is measured by constructing and fitting an individual “template.” Because each template is unique, it necessarily has lower S/N than an ePSF determined from many stars.

Exploiting the Galactic bulge stars along the line of sight to Sagittarius, Pryor et al. (2010) derived an absolute proper motion for this galaxy by measuring its proper motion relative to bulge stars and by determining the absolute proper motion of the bulge stars using the absolute proper motion of the Galactic center itself (Reid & Brunthaler 2004). This method requires a target that is close in projection to the Galactic center. Many Galactic globular clusters satisfy this requirement.

The current article derives the absolute proper motion of the Draco dwarf galaxy from HST data using both QSOs and compact galaxies as standards of rest and compares the results obtained with the two methods. Table 1 lists those properties of Draco that were used in deriving its space motion.

The rest of this article is organized as follows. Section 2 describes the observations and data and Section 3 explains the process of deriving the proper motion. Section 4 presents results and Section 5 contains a summary and discussion.

2. Observations and Data

We obtained first-epoch images for three distinct pointings in the direction of Draco using the Advanced Camera for Surveys (ACS) and Wide Field Channel (WFC) combination on HST in cycle 13. For each pointing, WFC1 is centered on a spectroscopically-confirmed QSO. Ideally, second-epoch imaging would be obtained with the same detector. However, only one pointing was imaged in cycle 15 before the failure of ACS; the failure forced the other two to be imaged with the Wide Field and Planetary Camera 2 (WFPC2). Table 2 summarizes the observations, with column 1 giving the name of the pointing and columns 2 and 3 the celestial coordinates of the QSO. The dates of the observations are in column 3: the upper one is for the first epoch and the lower for the second; their difference is the time baseline. It is about 3 years for Dra 1 and Dra 3 and about 2 years for Dra 2. The final three columns list the detector, filter, and exposure time.

The second-epoch data taken with PC2 have a smaller field of view and worse charge-transfer efficiency (CTE) than the first-epoch data taken with ACS. The Dra 1 and Dra 3 fields have 16 and 9 stars with $S/N > 20$, respectively, on the PC chip with the QSO. These numbers of stars are, at best, only marginally sufficient to derive a proper motion. Another problem is that the correction for the effects of the degrading CTE of WFPC2, which produces shifts in the positions of stars comparable to those from the proper motions (Bristow et al. 2005), must also be derived from these few stars. Thus, obtaining reliable proper motions for these fields proved impossible. Kallivayalil et al. (2013) similarly decided that their WFPC2 data were not useful for measuring the proper motion of the Magellanic Clouds. The data from Dra 1 and Dra 3 are not considered further in this article, though we note that obtaining a second epoch for these pointings with the repaired ACS would likely reduce the uncertainty in the proper motion of Draco by more than a factor of five.

Figure 1 shows the locations of the WFC1 and WFC2 fields of the Dra 2 pointing on a 20×20 arcmin section of the sky from the STScI Digitized Sky Survey². The dashed ellipse

²The Digitized Sky Surveys were produced at the Space Telescope Science Institute under U.S. Government grant NAG W-2166. The images of these surveys are based on photographic data obtained using the Oschin Schmidt Telescope on Palomar Mountain and the UK Schmidt Telescope. The plates were processed into the present compressed digital form with the permission of these institutions. The Second Palomar

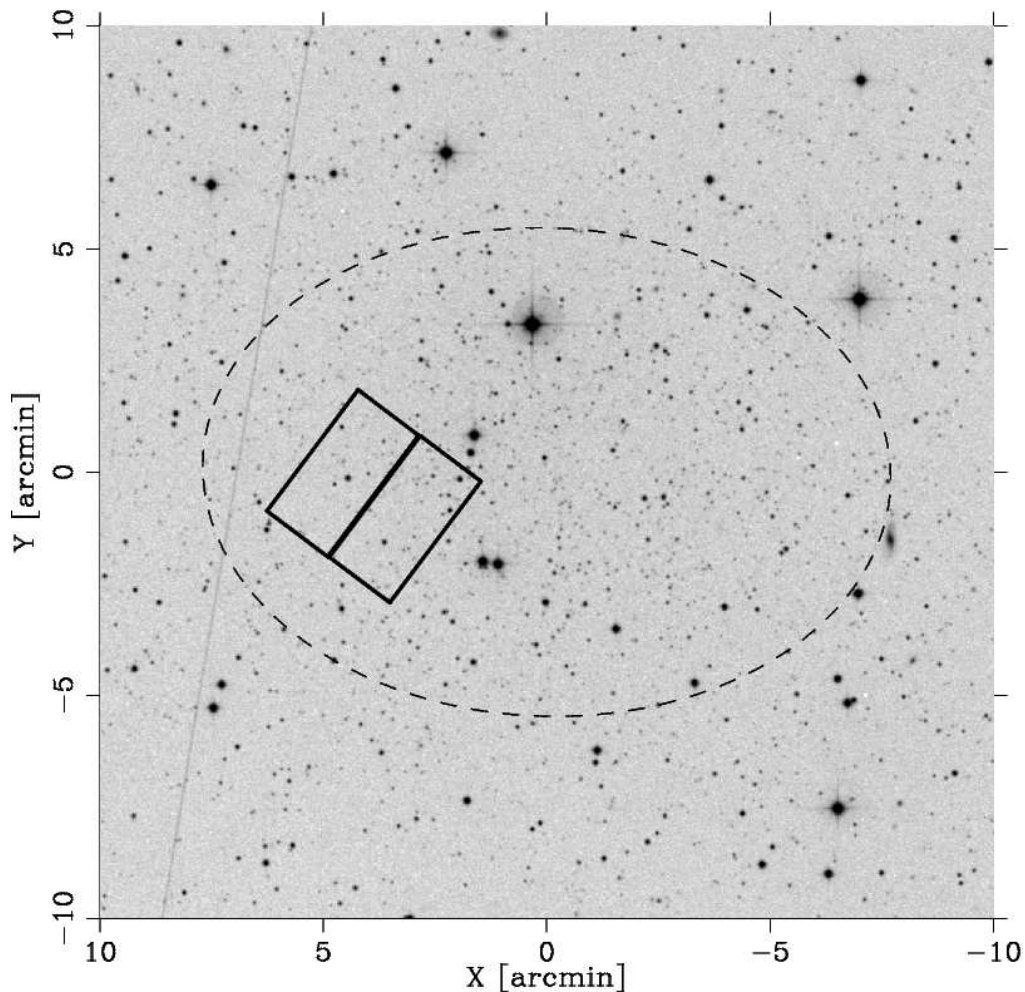


Fig. 1.— Locations of the WFC1 and WFC2 fields of the Dra 2 pointing on a 20×20 arcmin section of an image of the sky centered on Draco. North is up and East is to the left. The most eastward field is WFC1. The dashed ellipse delineates the core of Draco. The values for Draco’s center, position angle, ellipticity, and core radius are from Table 1.

delineates the core of Draco. The top-left panel of Figure 2 is the average, with cosmic rays rejection, of the 19 images of the WFC1 field taken at the first epoch. The QSO is at the center of a 600×600 pixel² box and an arrow points at it. The smaller top-right panel depicts the region of the image within the box, with the arrow again pointing at the

Observatory Sky Survey (POSS-II) was made by the California Institute of Technology with funds from the National Science Foundation, the National Geographic Society, the Sloan Foundation, the Samuel Oschin Foundation, and the Eastman Kodak Corporation.

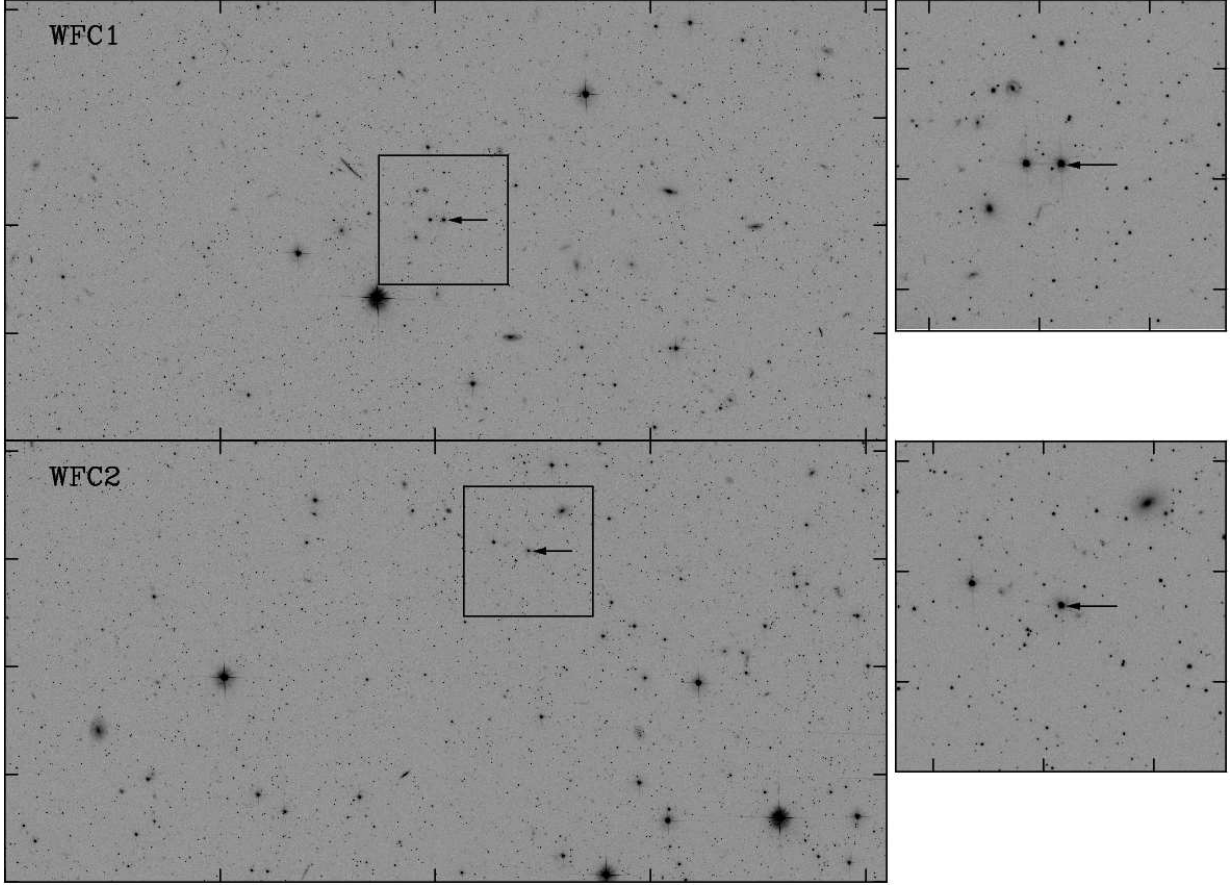


Fig. 2.— Top-left panel: the average of the 19 images taken at the first epoch, with cosmic rays rejected, for the WFC1 field. The arrow points to the QSO, which is at the center of the 600×600 pixel² box. In the chronologically first exposure, the QSO is at $(x, y) = (2039.60, 1025.04)$ pixel. The smaller top-right panel depicts the region of the image within the box; again, the arrow points to the QSO. The bottom two panels are analogous images for the WFC2 field. Examination of candidate compact galaxies revealed the presence of a likely QSO at $(x, y) = (2432.53, 1536.54)$ pixel.

QSO. Table 2 lists the coordinates of the QSO, which was discovered by Kinemuchi et al. (2008, their object 264). It has $V = 19.86$ and $V - I = 0.40$ (Kinemuchi et al. 2008), $g = 20.29$ and $g - r = 0.29$ (Ahn et al. 2012, SDSS DR9), and a redshift of 0.9465 (H. C. Harris, private communication). Similarly, the bottom two panels are for the WFC2 field. The arrow points to an object which we identified as a likely QSO on the basis of visual inspection, photometry (Richards et al. 2009), and association with an X-ray source (Flesch 2010). It is at $(\alpha, \delta) = (17 : 20 : 43.10, +57 : 54 : 43.0)$ (J2000.0) and has $g = 20.93$ and $g - r = 0.49$ (Ahn et al. 2012, SDSS DR9).

3. Data Reduction and Analysis

3.1. Measuring Coordinates

Deriving a proper motion of a resolved stellar system such as Draco requires accurate measurements of the coordinates of both the member stars and the zero-point objects — here QSOs and compact galaxies. The following are the steps in measuring these coordinates.

1. Correct all of the exposures for the degrading charge transfer efficiency using the standard pipeline processing of ACS images, which eliminates the need for any further corrections for this effect.
2. Determine the first estimate of an object’s coordinates and magnitude using the stand-alone software package DOLPHOT (Dolphin 2000). There are 19 dithered exposures at each epoch and, thus, this step gives 19 locations for an object — one per exposure — in the coordinate system of the CCD. Because the exposures are dithered, the locations can differ by several to a few tens of pixels.
3. Match the same objects across the exposures, determine the coefficients of the most general quadratic transformation between the first exposure and each of the subsequent exposures, and transform the coordinates from those subsequent exposures to the coordinate system of the first exposure. These tasks are all done using the DAOPHOT software package (Stetson 1987, 1992, 1994). From now on in this article, the “fiducial coordinate system” refers to that of the chronologically first exposure in an epoch.
4. Construct a combined image with higher S/N and no cosmic rays or hot pixels from the 19 exposures and the coordinate transformations using only integer-pixel shifts. The combined image has the same location and number of pixels as the fiducial image.
5. Discriminate between stars and compact galaxies in both the WFC1 and WFC2 fields using the FWHM of objects found by SExtractor (Bertin & Arnouts 1996) in the combined image. For every object with a FWHM greater than 2.5 pixel — a likely galaxy — and a S/N greater than 15, construct a sub-sampled image on a 65×65 array of a 13×13 pixel² cutout using the same methods described by Piatek et al. (2002b). Visually inspect each sub-sampled image to reject objects that are close pairs of stars, stars superimposed on nebulosity or a galaxy, and galaxies that are too extended to yield accurate locations.
6. Construct a stellar ePSF that is independent of location in the image and averaged over all exposures in both epochs using stars with a S/N greater than 40. Anderson & King (2000) and in Piatek et al. (2002b) give the specifics of the construction.

7. Construct an individual template for each identified galaxy and QSO that is averaged over all exposures in both epochs using a method similar to that described in Mahmud & Anderson (2008) and Sohn et al. (2012). The template is a two-dimensional function that represents the distribution of light in the galaxy convolved with the ePSF. The initial center of the template is the brightest pixel of the galaxy, which is not necessarily the geometric center of its image. The ePSFs for stars and templates for galaxies are determined by interpolation in a 25×25 grid of values for a 5×5 -pixel² region.
8. Measure the location in every exposure for every star and galaxy using the generated ePSFs and templates. Correct the coordinates for the known geometric distortion (Anderson 2006), derive the most general linear transformation between the fiducial coordinate system and those of the remaining exposures of an epoch, and average the transformed coordinates at each epoch to produce a final location and uncertainty. At the end of this step an object has two sets of coordinates, one in the fiducial coordinate system of each epoch.

The above procedure produces coordinates for the set of objects common to the two epochs: the QSO, 97 selected galaxies, and 1840 stars with S/N greater than 10 in the WFC1 field and the QSO, 82 selected galaxies, and 2209 stars with S/N greater than 10 in the WFC2 field. Figure 3 depicts for the WFC1 field the gray-scale maps (top panels) and their corresponding constant-brightness contours (bottom panels) of, from left to right, the average stellar ePSF and the templates of the QSO, the brightest galaxy (S/N = 196,

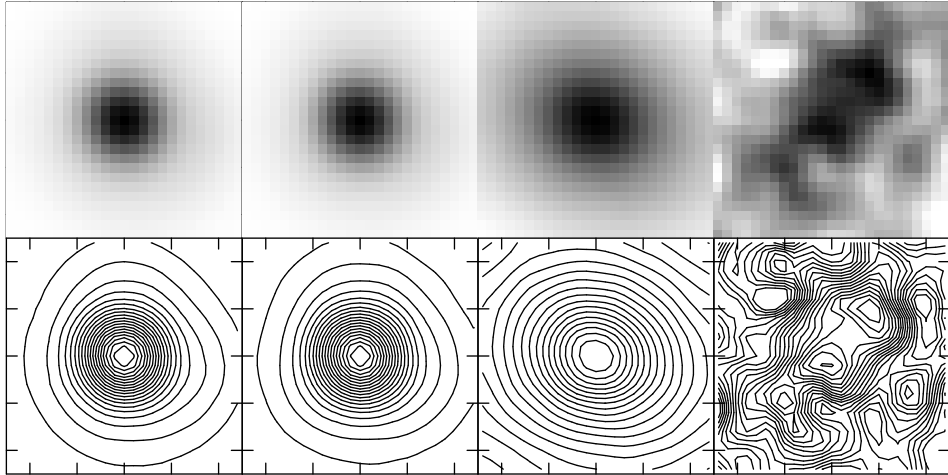


Fig. 3.— Gray-scale maps (top row of panels) and the corresponding constant-brightness contours (bottom row of panels) of, from left to right, the average stellar ePSF and the templates of the QSO, the brightest galaxy, and the faintest galaxy in the WFC1 field.

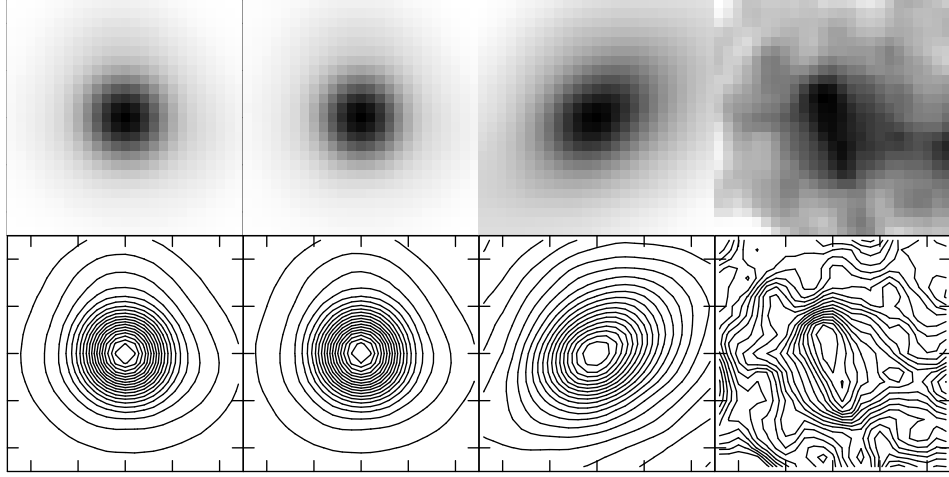


Fig. 4.— The same as Figure 3 for the WFC2 field.

FWHM = 5.5 pixel), and the faintest galaxy ($S/N = 9.4$, FWHM = 6.3 pixel). Similarly, Figure 4 depicts for the WFC2 field, from left to right, the average stellar ePSF and the templates of the QSO, the brightest galaxy ($S/N = 138$, FWHM = 4.0 pixel), and the faintest galaxy ($S/N = 9.9$, FWHM = 4.9 pixel). Note that the above values for the S/N are calculated only using pixels in the 5×5 pixels² array, while the values for the FWHM are calculated by SExtractor for the entire galaxy and may not measure the width of compact core.

Figures 3 and 4 show that, for both fields, the template of the QSO is nearly identical to the stellar ePSF. Thus, the results reported in the rest of this article are derived by fitting the stellar ePSF to the images of the QSOs. This approach allows a direct comparison between the technique that measures a proper motion using a QSO as the astrometric zero-point, such as Piatek et al. (2002b), and that which uses galaxies. The proper motions derived from the QSOs by fitting their templates do not differ significantly from those derived by fitting the ePSF in either value or the size of the uncertainty.

The uncertainty in the location of an object, as estimated from the scatter of the transformed coordinates around the mean, depends approximately linearly on $(S/N)^{-1}$, as shown in Figure 5 and 6 for the WFC1 and WFC2 fields, respectively. The slanted crosses in the figures are for stars and the open circles are for galaxies, with the size of the circle proportional to the FWHM. The plots show that the positional uncertainty for the stars with the highest S/N is about 0.01 pixel and this increases to 0.05 pixel at a S/N of 20. Galaxies have larger uncertainties than stars at a given S/N , as expected from their larger FWHMs.

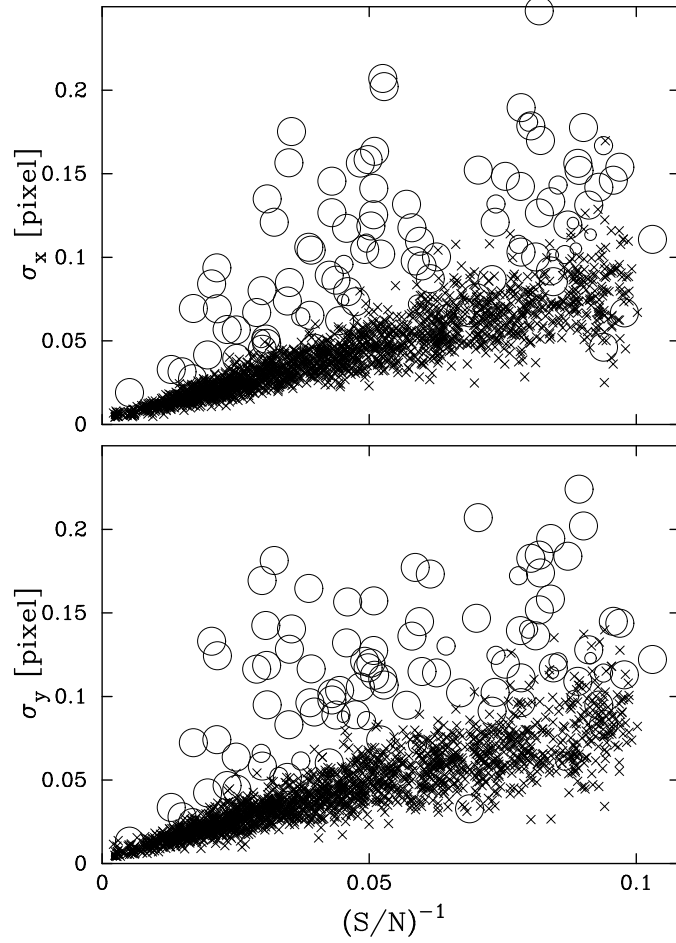


Fig. 5.— The rms scatter around the mean of the X-component (top panel) and the Y-component (bottom panel) of the centroid as a function of $(S/N)^{-1}$ for the first epoch exposures and WFC1 field. The slanted crosses are for stars and open circles for galaxies, with the size of the circle proportional to the FWHM.

3.2. Measuring the Proper Motion

The procedure for measuring the proper motion of Draco used in this paper is similar to that in our previous work (e.g., Piatek et al. 2002b). In that work, the stars of the galaxy determine a comoving coordinate system in the reference frame of the first epoch that we call the standard coordinate system. Average coordinates in the fiducial system of the second epoch are transformed into the standard system using the most general quadratic

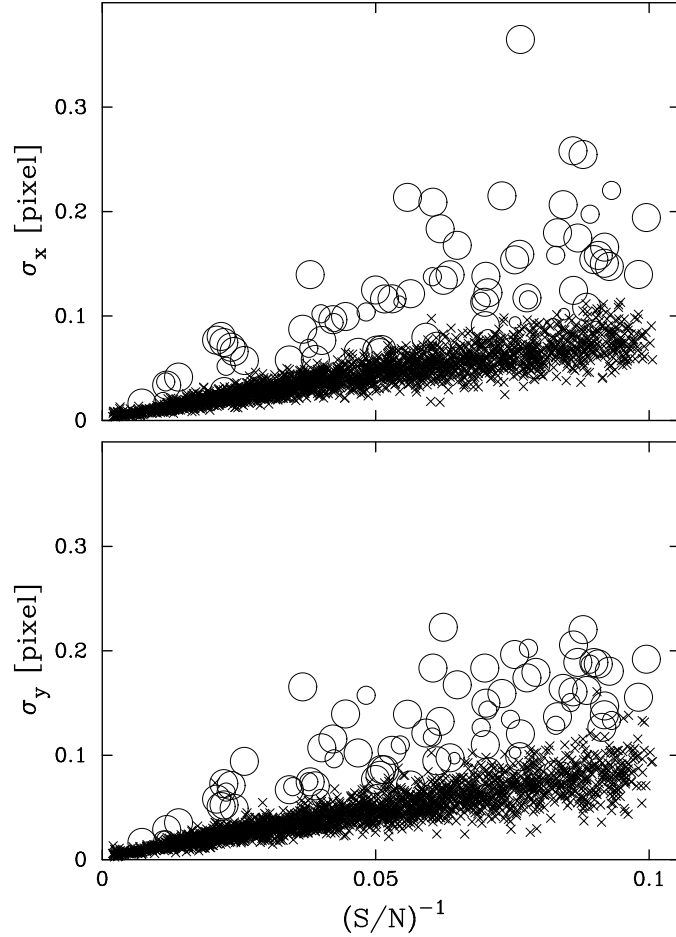


Fig. 6.— The same as Figure 5, except with a different vertical scale, for the WFC2 field.

transformation, which in the current work needed to be supplemented by adding the term x^3 to eliminate an obvious trend in the residuals. In the standard coordinate system, the stars of the galaxy are at rest, whereas the QSO (and field stars) are moving. The reverse of the motion of the QSO in the standard coordinate system is the proper motion of the galaxy.

In the current work, background galaxies are treated like the QSO was previously and, thus, the proper motion of Draco is the reverse of the average motion of the galaxies in the standard coordinate system. Although the background galaxies are numerous enough to determine a fixed coordinate system at both epochs, the more numerous and better-measured stars of Draco determine a more accurate standard coordinate system. In both the previous

and current work it is necessary to increase the uncertainties of the average coordinates at the two epochs to produce a chi-square (χ^2) of one for the transformation of the coordinates between the two epochs. The current data favor making this increase by adding a constant in quadrature to the uncertainties over multiplying them by a constant, as was done in our previous work. The additive constant is 0.0048 pixel for the WFC1 field and 0.0046 pixel for the WFC2 field.

The standard coordinate system is co-moving with Draco. Let μ_x and μ_y be the x and y components, respectively, of the motion (in pixel yr⁻¹) of an object in this coordinate system. Thus, a star of Draco should have (μ_x, μ_y) consistent with zero, whereas the field stars, background galaxies, and the QSOs have a non-zero motion. It is possible for a field star to have $(\mu_x, \mu_y) = (0, 0)$ pixel yr⁻¹ if its proper motion is the same as that of Draco, though this is an unlikely occurrence. The set of stars that determine the standard coordinate system results from iteratively rejecting stars whose μ_x or μ_y differ from zero by a statistically significant amount.

Figure 7 shows for the WFC1 field μ_x (top panels) and μ_y (bottom panels) as a function of S/N for (left panels) the likely stars of Draco and the QSO and (right panels) the background galaxies, field stars, and – again – the QSO. A plus symbol represents a likely star of Draco, a filled star the QSO, a filled triangle a background galaxy, and an open circle a field star. Figure 8 is the corresponding plot for the WFC2 field. In both figures, the plots for the likely stars of Draco show that their mean motion in the standard coordinate system, $(\langle \mu_x \rangle, \langle \mu_y \rangle)$, is consistent with zero, albeit with a scatter that increases with decreasing S/N. The plots for the other objects show that there are bright field stars with values for (μ_x, μ_y) that are, by construction, significantly different from zero. The points for the background galaxies have larger error bars and show a greater scatter than the stars of Draco with the same S/N. They should not show any systematic trends with S/N but the large scatter and the scarcity of galaxies makes this assessment difficult.

The four panels in Figure 9 plot μ_x and μ_y as a function of the location X and Y in the detector for the WFC1 field. Figure 10 is the same plot for the WFC2 field. The likely stars of Draco (plus symbols) are stationary in this system and, thus, the points should scatter around 0 pixel yr⁻¹ and show no trends with either X or Y , which is the case. Although the galaxies (filled triangles) are not at rest in the standard coordinate system, their motions should scatter around some mean value and show no trends with either X or Y . A visual inspection of the plots does not show any alarming trends with position; however, the number of galaxies is small. Similarly, the field stars (open circles) do not have to scatter around zero and would be unlikely to show trends across the field.

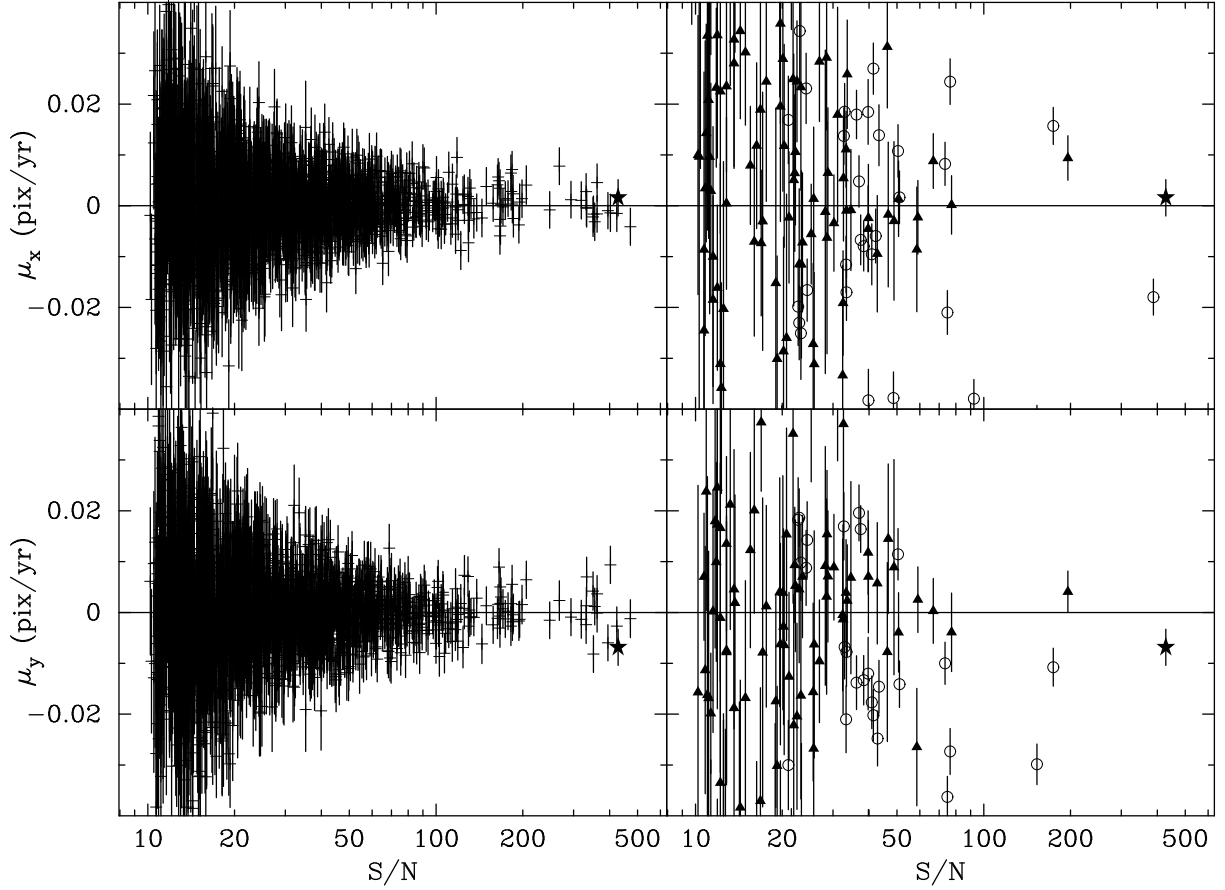


Fig. 7.— Motion in the standard coordinate system, μ_x and μ_y , in pixel yr^{-1} as a function of S/N for the WFC1 field. The panels on the left are for the likely stars of Draco (plus symbols) and the QSO (filled star), while those on the right are for the galaxies (filled triangles), field stars (open circles), and - again - the QSO. Only field stars with S/N greater than 20 are shown.

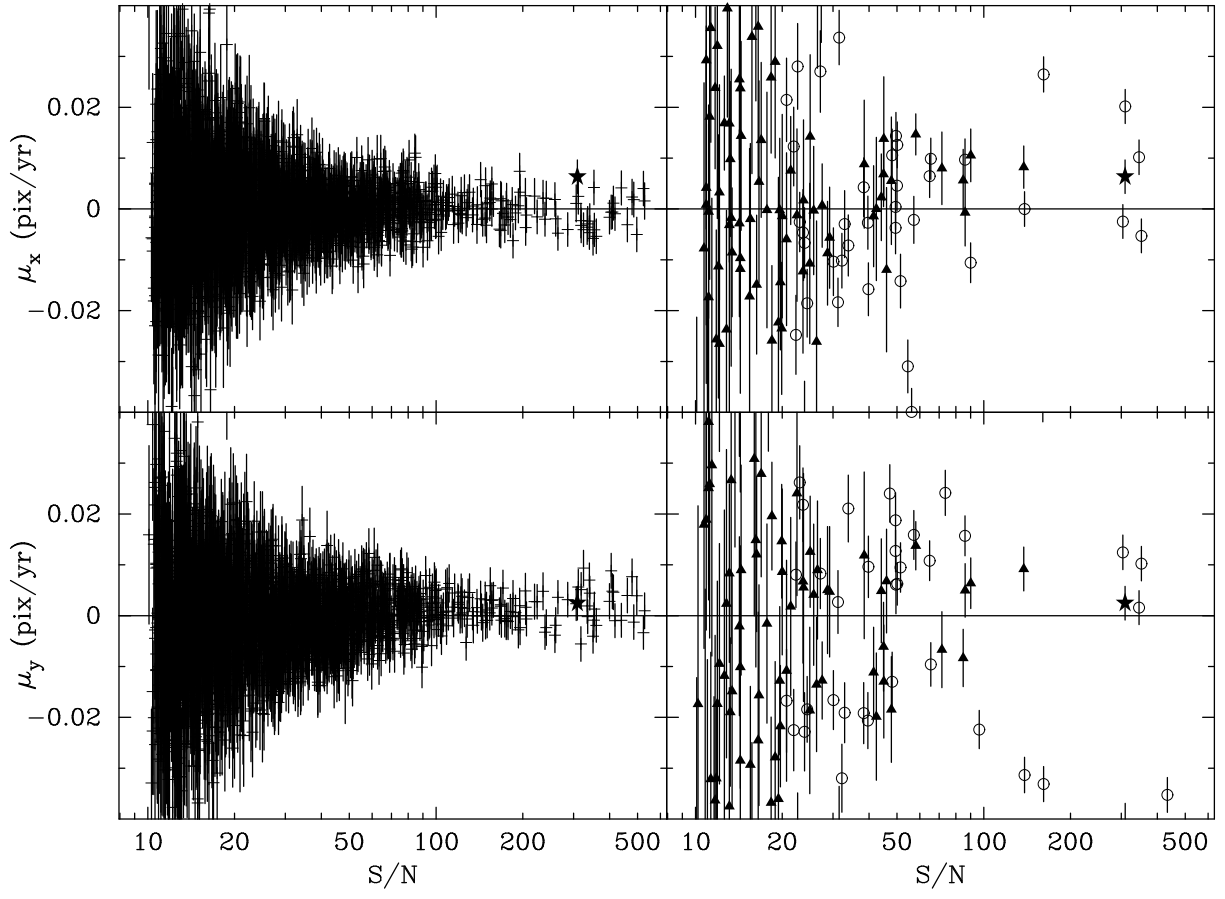


Fig. 8.— The same as Figure 7 for the WFC2 field.

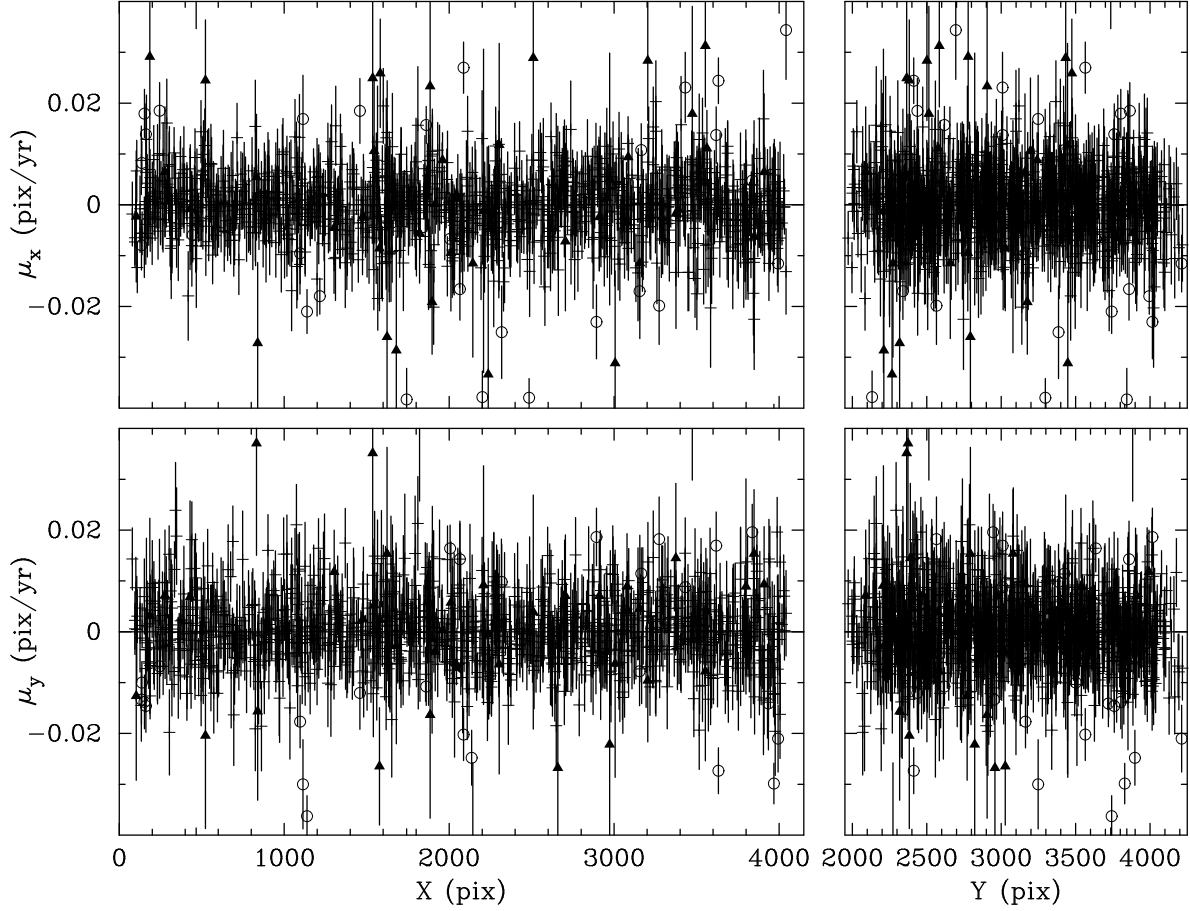


Fig. 9.— Motions in the standard coordinate system, μ_x and μ_y , in pixel yr^{-1} as a function of X (left panels) and Y (right panels) for the WFC1 field. The plus symbols represent the likely stars of Draco, filled triangles galaxies, open circles field stars, and the filled star the QSO. There are no obvious trends with either X or Y for any class of object.

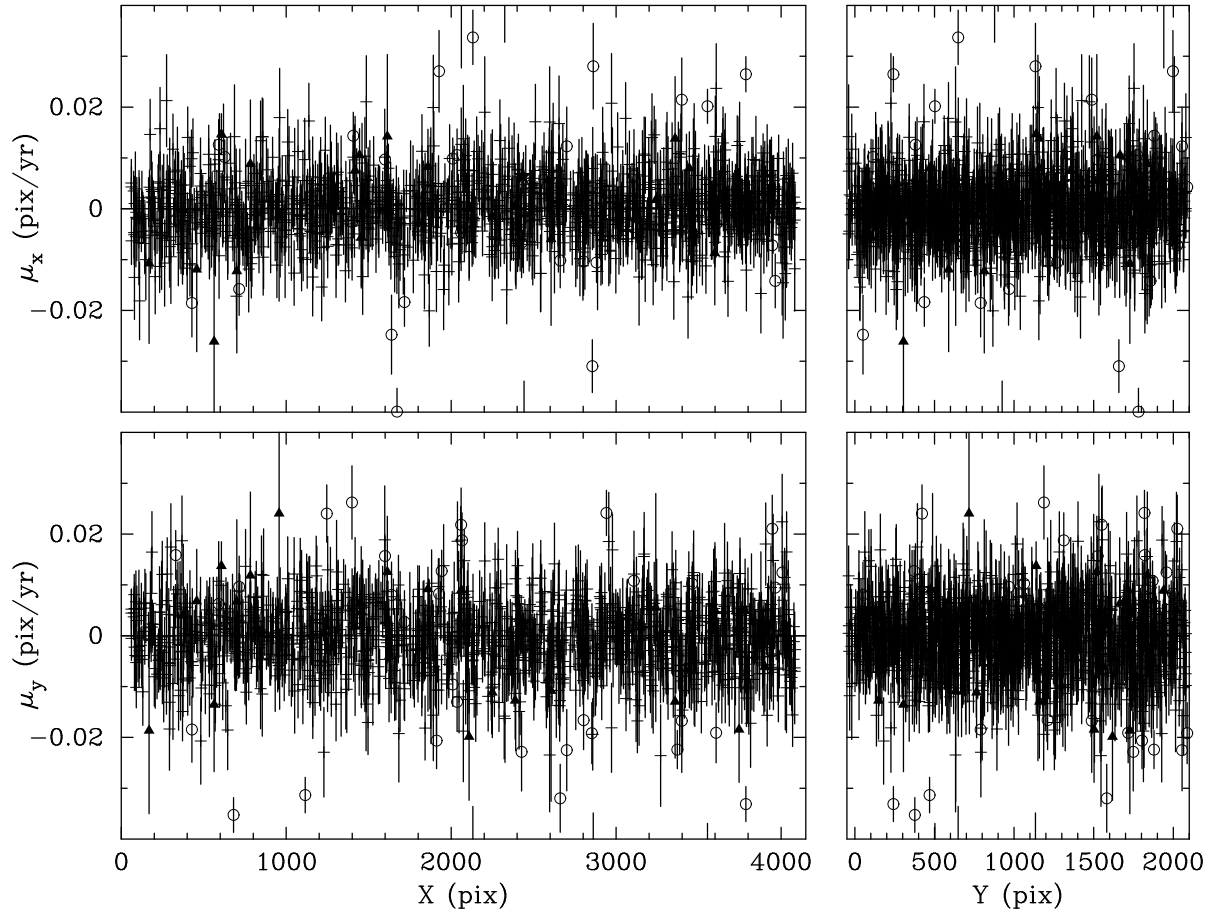


Fig. 10.— The same as Figure 9 for the WFC2 field.

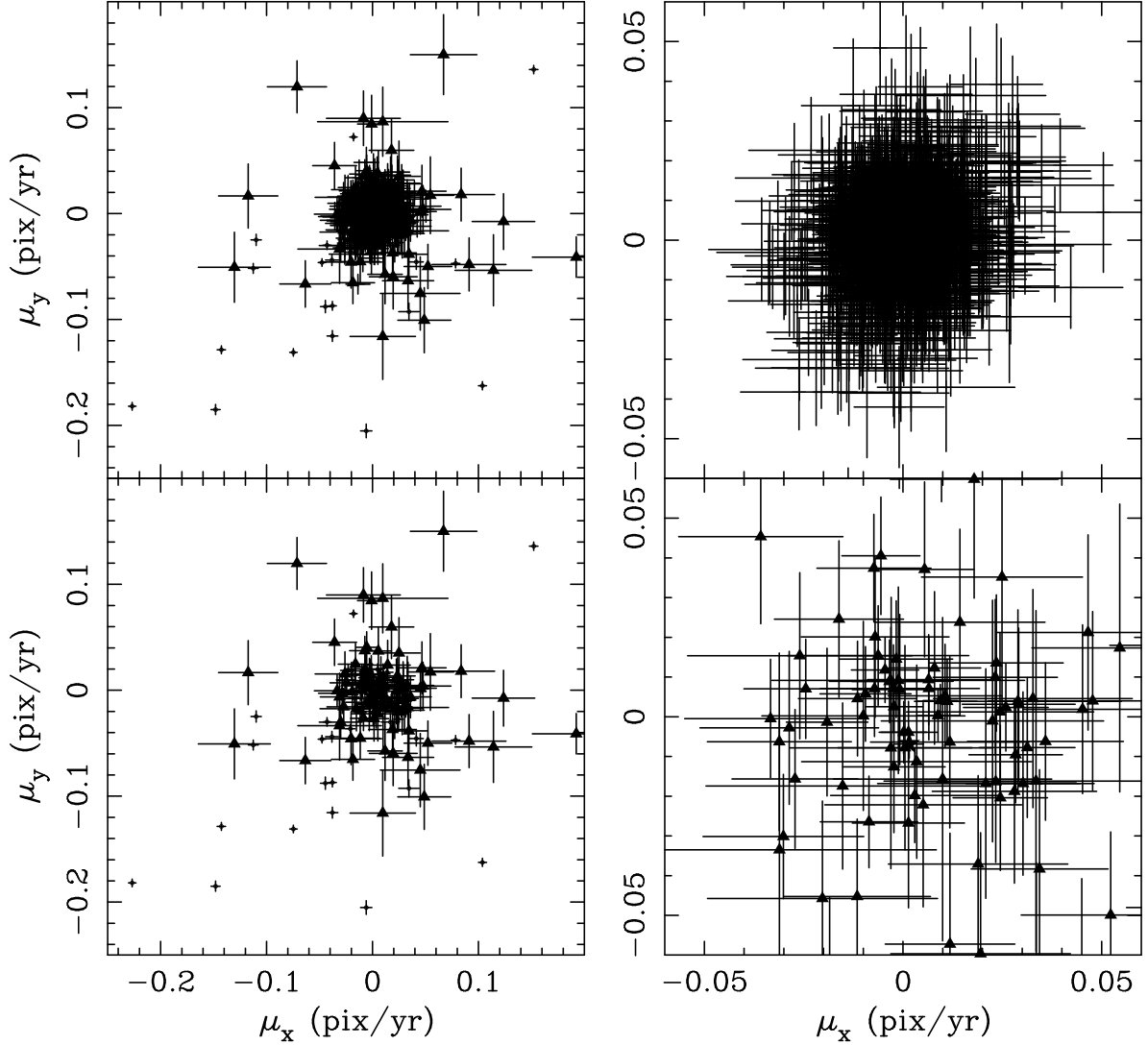


Fig. 11.— The distribution of the measured motions in the standard coordinate system, (μ_x, μ_y) , in pix yr^{-1} for the objects in the WFC1 field. A plus symbol represents a likely star of Draco, the filled star the QSO, a filled triangle a galaxy, and an open circle a field star. Top-left panel: the distribution for all of the objects. Top-right panel: that for the likely stars of Draco. Bottom-left panel: That for the QSO, galaxies, and background stars with the scale the same as that in top-left panel. Bottom-right panel: that for the QSO and galaxies with the scale the same as that in the top-right panel.

Figures 11 and 12 show the distribution of measured values of (μ_x, μ_y) for the WFC1 and WFC2 fields, respectively. The symbols have the same meaning as in the previous four figures, though the circles representing field stars have been reduced in size to deemphasize these objects. In each figure, the top-left panel shows the distribution for all of the objects (note the different scales for the two fields). The likely stars of Draco tightly and symmetrically clump around $(\mu_x, \mu_y) = (0, 0)$ pix yr⁻¹. The galaxies cluster around a point that cannot be distinguished from $(0, 0)$ pix yr⁻¹ at the scale of these plots. The field stars need

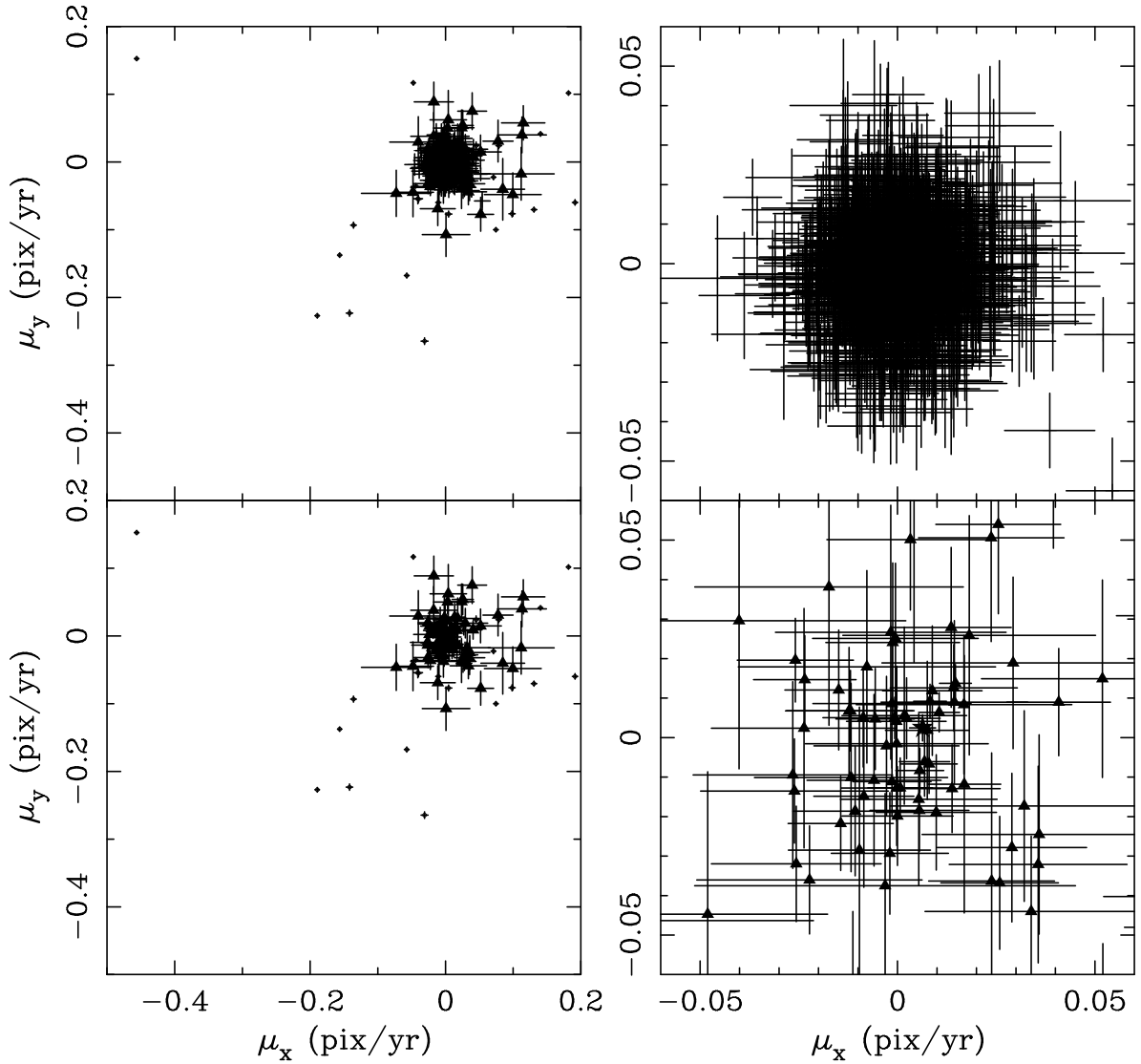


Fig. 12.— The same as Figure 11 for the WFC2 field.

not scatter around the origin and visual inspection confirms this. The top-right panels in Figures 11 and 12 show the distribution for the likely stars of Draco. If only random errors are present, the distribution should be isotropic with the density of points increasing towards the origin; both panels show this. The bottom-left panels depict the distribution for the galaxies and field stars. They show more clearly the clumping of the galaxies around a point close to the origin. Finally, the bottom-right panels are zoomed-in views of the distribution for the galaxies only (including the QSO).

Each of the two fields yields two measurements of the proper motion of Draco, one based on the motion of the QSO in the standard coordinate systems and the other based on the weighted average motion of the galaxies in those systems. The weighted average is $(\langle\mu_x\rangle, \langle\mu_y\rangle) = ((-5.6 \pm 2.2) \times 10^{-3}, (-0.4 \pm 2.4) \times 10^{-3})$ pixel yr⁻¹ for the 97 selected galaxies in the WFC1 field and $((-6.7 \pm 1.9) \times 10^{-3}, (-0.4 \pm 2.0) \times 10^{-3})$ pixel yr⁻¹ for the 82 galaxies in the WFC2 field. The motions for the QSOs in the standard coordinate systems are $((-1.6 \pm 3.6) \times 10^{-3}, (6.9 \pm 3.6) \times 10^{-3})$ pixel yr⁻¹ and $((-6.3 \pm 3.3) \times 10^{-3}, (-2.4 \pm 3.3) \times 10^{-3})$ pixel yr⁻¹ for the WFC1 and WFC2 fields, respectively. The average motion of the galaxies and the motion of the QSO within a field are directly comparable. Because the WFC1 and WFC2 detectors have nearly the same orientation and have the same readout direction, the two standard coordinate systems are nearly the same and, thus, motions in the two fields can also be compared.

The weighted average motion of the galaxies in a field does not change significantly when the sample is reduced based on S/N. The scatter of the individual measured motions around their mean is greater than expected from the uncertainties derived from those of the measured positions at the two epochs, implying that the uncertainties in the motions are too small. The origin of this underestimate is difficult to determine, therefore we have taken the empirical approach of increasing the uncertainties in the motions by a multiplicative factor until the χ^2 of the scatter around the mean is one. A multiplicative increase is preferred over increasing the uncertainty by adding a constant in quadrature because a single multiplicative factor is sufficient for all subsamples of galaxies selected by S/N, while a different value of the additive constant is needed for different subsamples. The multiplicative factor is 1.55 for the WFC1 field and 1.37 for the WFC2 field. The uncertainties in the weighted means given above include this increase.

3.3. Comparison of Measurement Uncertainties

The uncertainty in each component of the motion of a QSO is about 3.5×10^{-3} pixel yr⁻¹, implying that each coordinate of the position in the standard coordinate system has an accu-

racy of about 0.005 pixel at each epoch. This accuracy is comparable to the values of 0.003 – 0.007 pixel obtained using the PC2 and STIS cameras for QSOs in Sculptor (Piatek et al. 2006) and Fornax (Piatek et al. 2007). The fields in these galaxies have between 200 and 500 stars, enough that uncertainties in defining the standard coordinate system are negligible. The QSOs in the images for Draco have a higher S/N than those for Sculptor and Fornax by about a factor of two. That the positional uncertainty of a QSO is similar in all of these data argues that systematic errors are dominant over photon statistics and, indeed, all of these studies found it necessary to increase their uncertainties to account for such effects.

Sohn et al. (2013) measured the proper motion of Leo I from ACS/WFC images of a single pointing taken at two epochs separated by about 5 years using galaxies as the astrometric zero point. Their method of deriving the proper motion is similar, but not identical, to that used here. The data for Leo I consist of fewer but deeper images per epoch than that for Draco and, on average, have a total exposure time 1.7 times longer. Sohn et al. (2013) achieve an uncertainty in the proper motion that implies the average position of the galaxies is measured with an accuracy of 0.002 pixel at both epochs, whereas the corresponding uncertainty in the current study is 0.003 pixel. These uncertainties imply that the two studies are achieving comparable accuracies.

4. Results

Table 3 gives the four estimates of the proper motion of Draco in the equatorial coordinate system derived from each of the mean motions of the galaxies and of the QSOs from the previous section. These estimates and their uncertainties are shown in Figure 13. The weighted average of these values is shown as bold error bars and the value is given in the bottom line of Table 3 and Equation 1 below. This measured proper motion of Draco is the main result of the article:

$$(\mu_\alpha, \mu_\delta) = (17.7 \pm 6.3, -22.1 \pm 6.3) \text{ mas century}^{-1}. \quad (1)$$

The χ^2 of the scatter in the values of μ_α is 0.99 for three degrees of freedom. The probability of seeing a value of χ^2 this large or larger is 0.80. Similarly, the χ^2 for the values of μ_δ is 5.0, with a probability of 0.17. The agreement of the individual measurements with each other is acceptable and, thus, we conclude that the uncertainties in the measured proper motion are realistic.

The measured proper motion of Draco in the galactic coordinate system is

$$(\mu_\ell, \mu_b) = (-23.1 \pm 6.3, -16.3 \pm 6.3) \text{ mas century}^{-1}. \quad (2)$$

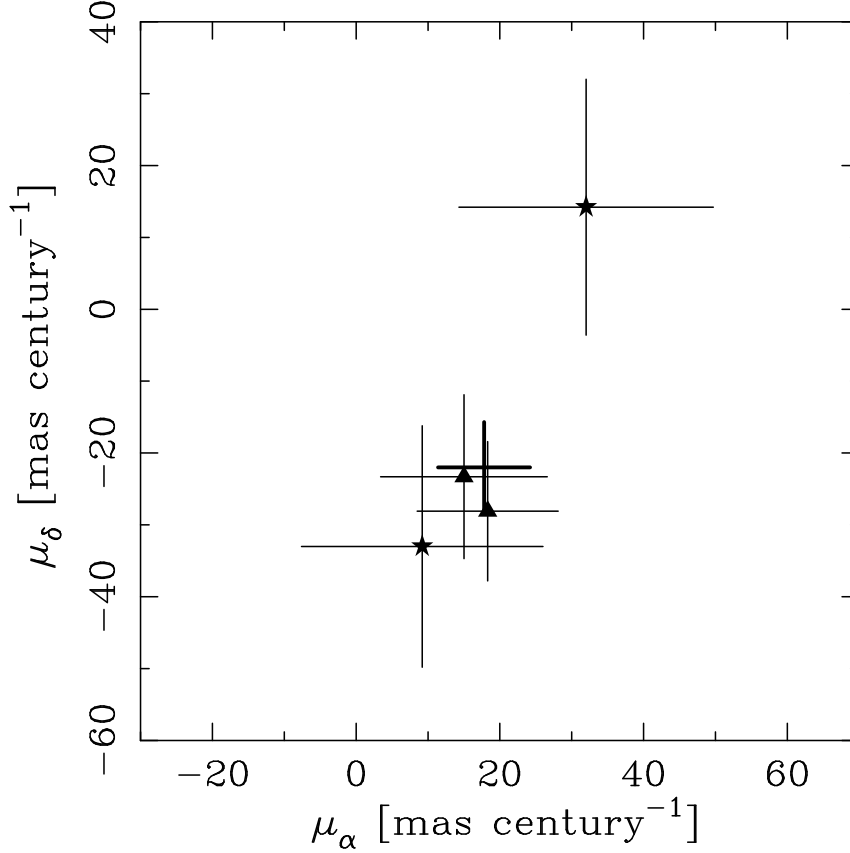


Fig. 13.— Comparison of four estimates of the proper motion of Draco. The filled triangles are the values derived using the mean motions of galaxies as the astrometric reference point, whereas the filled stars use the QSOs. The bold error bars show the weighted mean.

Converting the proper motion into the space velocity with respect to the Galactic center requires adopting values for the location and velocity of the Local Standard of Rest (LSR) and for the velocity of the Sun with respect to the LSR. To calculate these “Galactic rest frame” (Grf) quantities, we adopt a Galactocentric radius and velocity for the LSR of 8.0 kpc (*e.g.*, Eisenhauer et al. 2005; Ghez et al. 2008; Groenewegen et al. 2008) and 237 km s $^{-1}$ (consistent with the proper motion of the Galactic center from Reid & Brunthaler (2004)), respectively, and take the motion of the Sun with respect to the LSR to be $(u_\odot, v_\odot, w_\odot) = (-10.00 \pm 0.36, 5.25 \pm 0.62, 7.17 \pm 0.38)$ km s $^{-1}$ (Dehnen & Binney 1998), where the components are positive if u_\odot points radially away from the Galactic center, v_\odot is in the direction of the rotation of the Galactic disk, and w_\odot points in the direction of the North Galactic Pole. With these values and the heliocentric distance and radial velocity from Table 1, $(\mu_\alpha^{\text{Grf}}, \mu_\delta^{\text{Grf}}) = (51.4 \pm 6.3, -18.7 \pm 6.3)$ mas century $^{-1}$, $(\mu_\ell^{\text{Grf}}, \mu_b^{\text{Grf}}) = (-21.8 \pm 6.3, -50.1 \pm 6.3)$ mas century $^{-1}$, $(\Pi, \Theta, Z) = (27 \pm 14, 89 \pm 25, -212 \pm 20)$ km s $^{-1}$, and $V_r = -98.5 \pm 2.6$ km s $^{-1}$ and

$V_t = 210 \pm 25 \text{ km s}^{-1}$. The uncertainties in the above quantities come from Monte Carlo experiments based on the uncertainties in the measured proper motion and radial velocity, but not including that in the distance. The uncertainty in the distance from Table 1 would imply a total uncertainty in V_t of 29 km s^{-1} (determined by adding the 15 km s^{-1} contribution in quadrature). The contribution from the uncertainty in the distance has not been included because most of it is systematic uncertainty in the mean absolute magnitude of RR Lyrae variables as a function of metallicity (Kinemuchi et al. 2008).

The above velocities imply that Draco is moving towards the Galactic center at the present time on an orbit with an inclination to the Galactic plane of 70° , with a 95% confidence interval of $(59^\circ, 80^\circ)$. The position angle of the proper motion in the Galactic rest frame is $110^\circ \pm 7^\circ$, which is 22° from the position angle of the major axis given in Table 1. The difference between these angles suggests that the observed elongation of Draco is not in the plane of its orbit. Pawlowski et al. (2013) find that Draco is part of a planar distribution of satellite galaxies and estimate that the normal of the plane is in the direction $(\ell, b) = (169.5^\circ, -2.8^\circ)$ with an uncertainty of 0.43° . The velocity of Draco in our study implies that the direction of the orbital angular momentum vector is $(\ell, b) = (168.2^\circ \pm 4.6^\circ, -20.4^\circ \pm 5.5^\circ)$, which is consistent with an orbit within the plane (Pawloski & Kroupa 2013).

5. Summary and Discussion

We have measured the proper motion of the Draco dwarf galaxy using a single pointing imaged with ACS/WFC at two epochs separated by approximately two years. The main conclusions of this work are as follows.

1. Exposure times of $19 \times 430 \text{ s}$ per epoch provide enough compact galaxies in each of the WFC1 and WFC2 fields to give an astrometric zero point whose accuracy is comparable to that given by a single QSO.
2. The uncertainty in the proper motion achieved using the methods in this article is comparable to that achieved by Sohn et al. (2013) for Leo I using similar data, when account is taken of the different time baselines.
3. QSOs and background galaxies in each of the two fields all yield consistent measurements of the proper motion. The weighted mean of the four values is $(\mu_\alpha, \mu_\delta) = (17.8 \pm 6.4, -22.0 \pm 6.3) \text{ mas century}^{-1}$.
4. The plane of the orbit of Draco is consistent with the vast polar structure (VPOS) of Galactic satellites described by Pawlowski et al. (2013).

Scholz & Irwin (1994) used plates from the Palomar and Tautenburg Schmidt telescopes with a time baseline of about 35 years to measure a proper motion for Draco: $(\mu_\alpha, \mu_\delta) = (60 \pm 40, 110 \pm 50)$ mas century $^{-1}$. The value for μ_α agrees with our value within the uncertainties, but the value for μ_δ differs by more than twice the uncertainty.

An important use of the proper motions of the satellite dwarf galaxies is to provide a test of models for galaxy formation that is independent of the observed number and luminosities of these satellites. Lux et al. (2010) compared the known satellite orbits with those predicted by Λ CDM models and found that, while the observed orbits are more circular than predicted, the conflict is not severe. The study finds that a decisive test requires V_t 's accurate to about 10 km s $^{-1}$. Our measured V_t for Draco has an uncertainty of 25 km s $^{-1}$. Obtaining an additional epoch for any of the pointings in Table 2 with *HST* today would increase the time baseline by at least a factor of five and probably reduce the uncertainty in the proper motion by the same factor. With this additional epoch, the only obstacle to reducing the uncertainty in V_t below 10 km s $^{-1}$ would be the uncertainty in the distance. A similar outcome would result from an additional epoch for the other galaxies in Lux et al. (2010), which would increase the time baseline and reduce of the uncertainty in V_t by a factor of about seven.

CP and SP acknowledge the financial support of the Space Telescope Science Institute through the grants HST-GO-10229 and HST-GO-11697. EWO acknowledges support from the Space Telescope Science Institute through the grant HST-GO-10229 and from the National Science Foundation through the grants AST-0807498 and AST-1313006.

REFERENCES

- Ahn, C. P., Alexandroff, R., Allende Prieto, C., et al. 2012, *ApJS*, 203, 21
- Anderson, J. 2006, in *The 2005 HST Calibration Workshop*, ed. A. M. Koekemoer, P. Goud-frooij, & L. Dressel (Baltimore, MD: STScI), 11
- Anderson, J., & King, I. R. 2000, *PASP*, 112, 1360
- Armandroff, T. E., Olszewski, E. W., & Pryor, C. 1995, *AJ*, 110, 2131
- Bertin, E. & Arnouts, S. 1996, *A&AS*, 117, 393
- Bristow, P., Piatek, S., & Pryor, C. 2005, *ST-ECF Newsletter*, 38, 12
- Dolphin, A. E. 2000, *PASP*, 112, 1383
- Dehnen, W., & Binney, J. J. 1998, *MNRAS*, 298, 387
- Eisenhauer, F., et al. (2005), *ApJ*, 628, 246
- Flesch, E. 2010, *PASA*, 27, 283
- Ghez, A. M., et al. 2008, *ApJ*, 689, 1044
- Groenewegen, M. A. T., Udalski, A., & Bono, G. 2008, *A&A* 481, 441
- Kallivayalil, N., van der Marel, R. P., Besla, G., Anderson, J., & Alcock, C. 2013, *ApJ*, 764, 161
- Kinemuchi, K., Harris, H. C., Smith, H. A., Silbermann, N. A., Snyder, L. A., LaCluyzé, A. P., & Clark, C. L. 2008, *AJ*, 136, 1921
- Mahmud, N. & Anderson, J. 2008, *PASP*, 120, 907
- Milone, A. P., Villanova, S., Bedin, L. R., et al. 2006, *A&A*, 456, 517
- Lépine, S., Koch, A., Rich, R. M., & Kuijken K. 2011, *ApJ*, 741, 100L
- Lux, H., Read, J. I., & Lake, G. 2010, *MNRAS*, 406, 2312
- Odenkirchen, M., et al. 2001, *AJ*, 122, 2538
- Pawlowski, M. S. & Kroupa, P. 2013, *MNRAS*, 435, 2116
- Pawlowski, M. S., Kroupa, P., Jerjen, H. 2013, *MNRAS*, 435, 1928

- Piatek, S., Pryor, C., Armandroff, T. E., & Olszewski, E. W. 2002, *AJ*, 123, 2511
- Piatek, S., Pryor, C., Olszewski, E. W., Harris, H. C., Mateo, M., Minniti, D., & Tinney, C. G. 2002, *AJ*, 124, 3198
- Piatek, S., Pryor, C., Bristow, P., Olszewski, E. W., Harris, H. C., Mateo, M., Minniti, D., & Tinney, C. G. 2006, *AJ*, 131, 1445
- Piatek, S., Pryor, C., Bristow, P., Olszewski, E. W., Harris, H. C., Mateo, M., Minniti, D., & Tinney, C. G. 2007, *AJ*, 133, 818
- Pryor, C., Piatek, S., & Olszewski, E. W. 2010, *AJ*, 139, 839
- Reid, M. J., & Brunthaler, A. 2004, *ApJ*, 616, 872
- Richards G.T. Myers A.D., Gray A. G., et al. 2009, *ApJS*, 180, 67
- Sohn, S. T., Anderson, J., & van der Marel, R. P. 2010, in “The 2010 STScI Calibration Workshop: Hubble after SM4. Preparing JWST” Edited by Susana Deustua and Cristina Oliveira, p. 294
- Sohn, S. T., Anderson, J., & van der Marel, R. P. 2012, *ApJ*, 753, 7S
- Sohn, S. T., Besla, G., van der Marel, R. P., Boylan-Kolchin, M., Majewski, S., & Bullock, J. S. 2013, *ApJ*, 768, 139
- Scholz, R.-D., & Irwin, M. J. 1994, *Astronomy from Wide-Field Imaging* (IAU Symp. 161), ed. H. T. MacGillivray et al. (Dordrecht: Kluwer), 534
- Stetson, P. B. 1987, *PASP*, 99, 191
- Stetson, P. B. 1992, in *ASO Conf. Ser. Vol. 25, Astronomical Data Analysis Software and Systems*, ed. D. M. Worrall, C. Biemesderfer, & J. Barnes (San Francisco: ASP), 297
- Stetson, P. B. 1994, *PASP*, 106, 250

Table 1. Draco at a Glance

Quantity (1)	Value (2)	Reference (3)
Right Ascension, α (J2000.0)	17:20:18.1	Piatek et al. (2002a)
Declination, δ (J2000.0)	57:55:13	"
Galactic longitude, ℓ	86.3730°	
Galactic latitude, b	34.7088°	
Heliocentric distance	82.4 ± 5.8 kpc	Kinemuchi et al. (2008)
Position angle	$88^\circ \pm 3^\circ$	Odenkirchen et al. (2001)
Ellipticity, e	0.29 ± 0.02	"
Heliocentric radial velocity	-293.3 ± 1.0 km s ⁻¹	Armandroff, Olszewski & Pryor (1995)

Table 2. Information about Pointings and Images

Pointing (1)	R.A. (J2000.0) (2)	Decl. (J2000.0) (3)	Date $yyyy - mm - dd$ (4)	Detector (5)	Filter (6)	T_{exp} (s) (7)
Dra 1	17:19:34.4	57:58:49.8	2004 – 10 – 30	ACS/WFC	F555W	19×430
			2007 – 11 – 03	WFPC2/PC2	F555W	12×600
Dra 2	17:20:52.3	57:55:13.4	2004 – 10 – 19	ACS/WFC	F606W	19×430
			2006 – 10 – 15	ACS/WFC	F606W	19×427
Dra 3	17:21:48.3	57:58:05.4	2004 – 10 – 31	ACS/WFC	F606W	19×430
			2007 – 12 – 29	WFPC2/PC2	F606W	12×600

Table 3. Measured Proper Motion of Draco

Field (1)	μ_α (mas century ⁻¹) (2)	μ_δ (3)
WFC1 (QSO)	32.0 ± 17.7	14.2 ± 17.8
WFC1 (Galaxies)	15.0 ± 11.6	-23.3 ± 11.4
WFC2(QSO)	9.0 ± 16.5	-32.6 ± 16.4
WFC2 (Galaxies)	18.2 ± 9.6	-28.1 ± 9.6
Weighted mean	17.7 ± 6.3	-22.1 ± 6.3